# Microscopic calculations of nuclear level densities with the Lanczos method

*B. A. Brown*[1] *and W. E. Ormand*[2]
[1] Department of Physics and the National Superconducting Cyclotron Laboratory,
Michigan State University, East Lansing, MI 42284-1321, USA
[2] Lawrence Livermore National Laboratory, P.O. Box 808, L-414, Livermore, California 94551, USA

**Abstract**

A new method for computing the density of states in nuclei using an extrapolated form for the tri-diagonal matrix obtained from the Lanczos method is presented. This can be applied to configuration-interaction calculations with fully realistic nuclear Hamiltonians that are known to provide an excellent description of the low-lying structure of nuclei. This extrapolated Lanczos matrix (ELM) approach provides an accurate computation of the density of states up to the neutron separation energy for states that lie within the configuration space. Comparisons between theory and experiment for the average level density for $p$-wave resonances for iron isotopes using the $1p-0f$-shell model space and realistic nuclear Hamiltonians are shown. Also we show results for $J$-dependence of the level density and the total level density for negative-parity states.

The density of states is a fundamental property of nuclear structure that plays an important role in nuclear reactions. Of particular importance is the radiative capture of neutrons on short-lived nuclei, which through the r-process [1] in supernovae and neutron-star mergers [2], are thought to be responsible for the synthesis of the elements heavier than iron. Ideally, these reactions can be measured or constrained by experiment. Unfortunately, in most cases, the target nuclei are so short lived that direct measurement is infeasible, and the only alternatives are to rely on theoretical calculations or on indirect measurements, such as surrogates [3], which themselves reliant on theoretical input. Theoretical modeling requires an in-depth, and accurate description of the reaction processes, and in particular the density of states at or near the neutron decay threshold.

We report on a new microscopic framework to provide an accurate estimate of the level density for a variety of nuclei using an extension of the configuration-interaction approach with fully realistic nuclear Hamiltonians that are known to provide an excellent description of the low-lying structure of nuclei. We will exploit a universal property of the Lanczos algorithm, which will allow us to extrapolate the tri-diagonal Lanczos matrix elements beyond what is computationally viable, to accurately estimate the density of states within the shell-model configuration space. We demonstrate that the information needed to perform the extrapolation can be extracted from just the lowest 100 Lanczos iterations, thus, leading to a computationally efficient way to compute the density of states.

The principal goal behind nuclear-structure models is to find energy eigenvalues and wave functions for the nuclear Hamiltonian within a well-defined Hilbert space. The nuclear shell model starts with a set of $N$ many-body Slater determinants, $\mid \psi_i\rangle$, spanning the space to expand the full solution, i.e., $\mid \Psi\rangle = \sum_i c_i \mid \psi_i\rangle$. The coefficients $c_i$ are found by computing the matrix element $H_{ji} = \langle \psi_j \mid H \mid \psi_i\rangle$ and diagonalizing the resulting symmetric matrix. One of the most effective methods to find the eigenvalues is the Lanczos algorithm [4], which starts with an arbitrary vector $\mid v_1\rangle$ in the Hilbert space, and through successive operations of $\hat{H}$, $H_{ji}$ is reduced to tri-diagonal form with diagonal matrix elements, $\alpha$, and symmetric off-diagonal matrix elements, $\beta$. The energies and observables do not depend on the signs of the $\beta$ and they can be taken as positive.

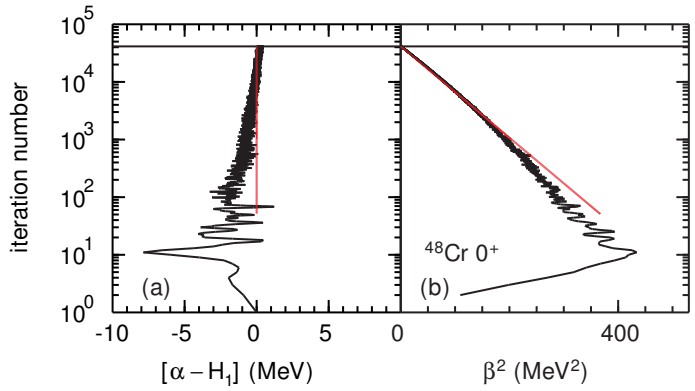


**Fig. 1:** TDME for $^{48}$Cr, $J = 0^+$, is the $pf$ model space. The black lines are the results of the exact calculation. The red lines correspond to the simplest approximation given by $\alpha_i = H_1$ and $\beta_i^2 = -(\sigma^2/2)z_i$.

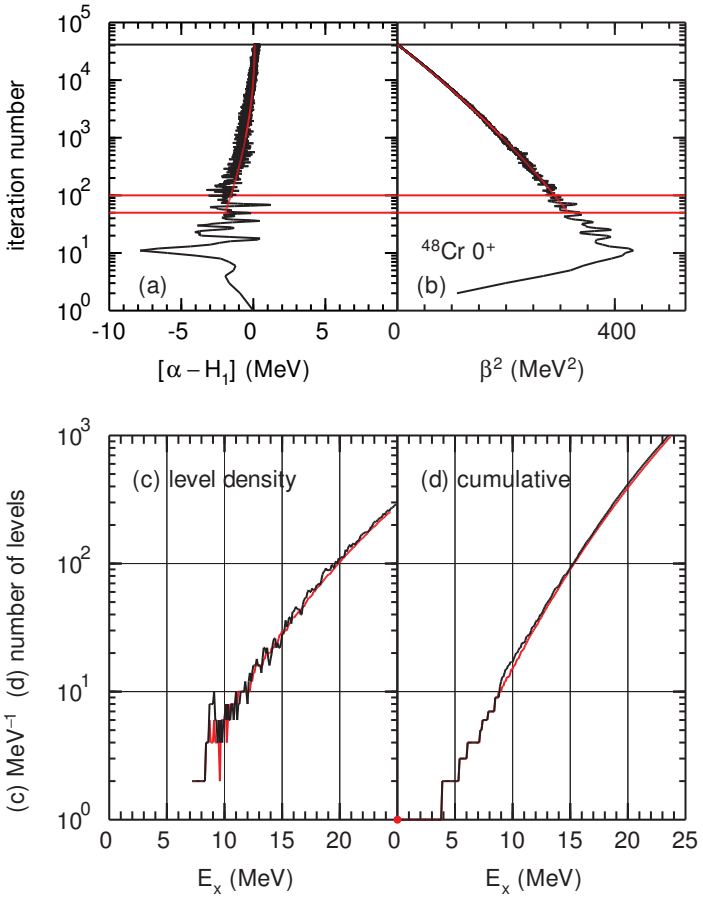


**Fig. 2:** (top) Tri-diagonal matrix elements (TDME) for $^{48}$Cr, $J = 0^+$, in the $pf$ model space. The black lines are the results of the exact calculations (same as in Fig. 1). The red lines are based on the ELM(100). (bottom) Level density with the exact calculation (black) compared to ELM(100) approximation (red).

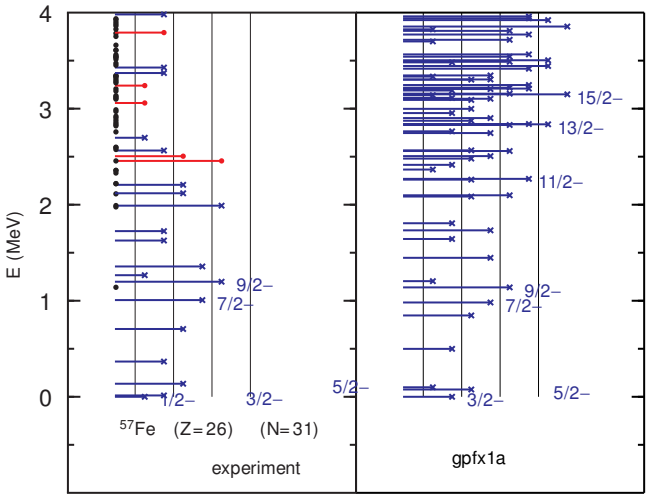


**Fig. 3:** Levels up to 3 MeV in excitation obtained with the GPFX1A Hamiltonian in the full $pf$ model space are shown in the right-hand side. The length of each line indicates the $J$ value. These are compared with the experimental energies from NNDC on the left-hand side. The blue lines are states with negative parity, and the red line are states with positive parity. If the spin-parity is uncertain it is shown as a black circle on the y axis.

Of particular interest is the behavior of the tri-diagonal matrix elements (TDME) with increasing iterations. The results for $^{48}$Cr are shown in Fig. 1. After several iterations, the diagonal elements, $\alpha_i$, are roughly constant and nearly equal to the first moment $H_1 = \mathrm{Tr}[\hat{H}] = (1/N_{dim}) \sum_i H_{ii}$, where $N_{dim}$ is the matrix dimension. At the same time, the off-diagonal elements, $\beta_i$, generally decrease to zero as $i \rightarrow N_{dim}$, and exhibit a Gaussian-like behavior $\beta_i = \sqrt{-(\sigma^2/2)\ln(i/N_{dim})}$ [6]. We rewrite this as $\beta_i^2 = b_1 z_i$, where

$$z_i = \ln(i/N_{dim}) \tag{1}$$

and $b_1 = -(\sigma^2/2)$ and $i$ is the iteration number. Thus, as in Fig. 1, when $i$ is plotted on a log scale vs $\beta_i^2$ the results are close to a straight line for large $i$ values.

At its core, the Lanczos algorithm is a moment method; efficiently computing $2n$ moments of $\hat{H}$ with respect to $\mid v_1\rangle$ after $n$ iterations. With $\mid v_1\rangle = (1/\sqrt{N_{dim}}) \sum_i \phi_i \mid \psi_i\rangle$, where $\phi_i$ is a random phase, we have

$$\alpha_1 = \frac{1}{N_{dim}} \sum_i H_{ii} + \sum_{i \neq j} \frac{\phi_i \phi_j}{N_{dim}} H_{ji}. \tag{2}$$

Thus, moments of $\hat{H}$ can be computed stochastically by selecting several random initial pivots and averaging. We find that for most cases with large $N_{dim}$, the remainder in Eq. 1 is generally small and of the order 1 keV. Under this condition, good estimates for the first two moments of $\hat{H}$ can be extracted from just the first Lanczos iteration, namely

$$H_1 \approx \alpha_1 \quad \text{and} \quad M_2 = \sigma^2 \approx \beta_1^2 \tag{3}$$

As an example, we consider the exact results for $^{48}$Cr, $J^\pi = 0^+$, obtained in the proton-neutron $pf$ basis. The states contain all possible values of isospin $T$. The dimension is $N_{dim} = 41,355$. The calculations were carried with the NuShellX [7] code, and with GPFX1A Hamiltonian [8]. The results for the exact results for the TDME for are shown in Fig. 1. They are compared with extrapolations based on $\alpha_i = H_1$ and $\beta_i^2 = -2M_2 z_i$. They give an approximation to the exact results above about 1000 iterations.

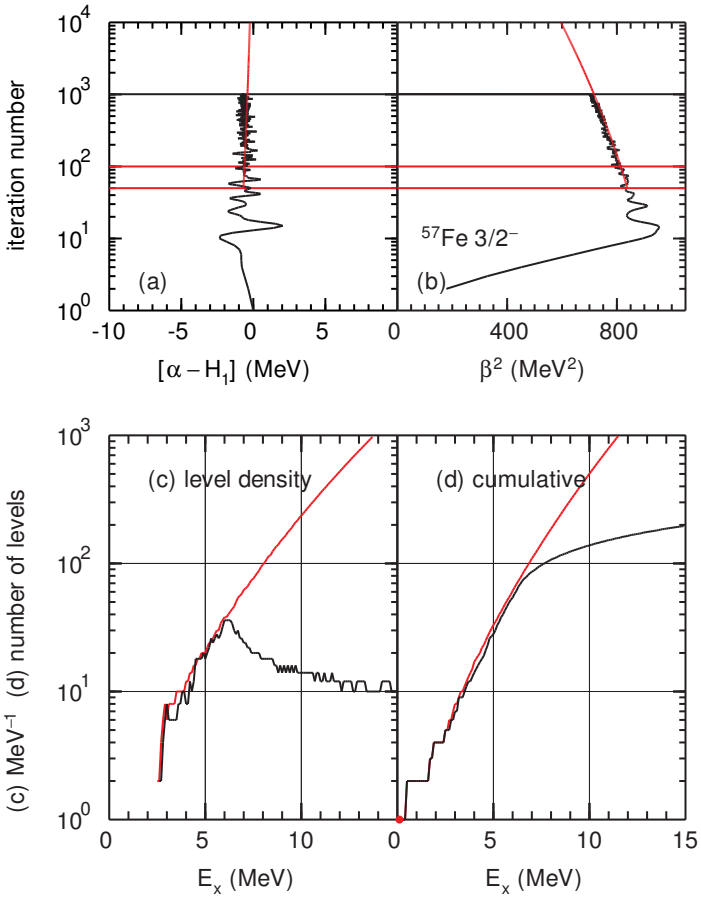


**Fig. 4:** (top) TDME for $^{57}$Fe, $J^\pi = 3/2^-$ in the $pf$ model space. The black lines are the results of the exact calculations. The red lines are based on the ELM(100). (bottom) Level density with the exact calculation (black) compared to ELM(100) approximation (red).

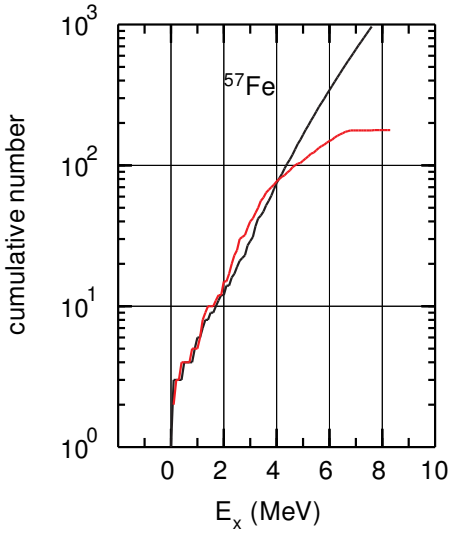


**Fig. 5:** The cumulative number of levels in $^{57}$Fe. The theoretical results for negative-parity states are shown by the black line. The experimental data from NNDC for all levels (both parity) is shown by the red line.

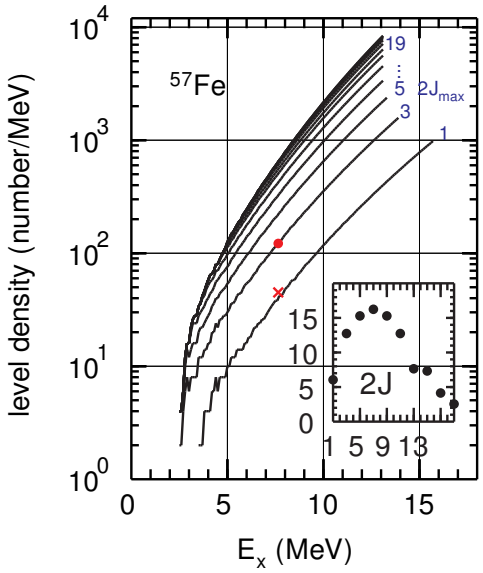


**Fig. 6:** Level density for negative parity states calculated for $^{57}$Fe. The lines show the cumulative level density up to the value of $2J_{max}$ as indicated on the right-hand side. The red dot is the $\ell$=1 experimental value for $J_{max} = 3/2^-$ at the neutron separation energy of $E_x = S_n = 7.65$ MeV [5]. The inset shows the percentage contribution to the total level density at $S_n$ for each $J$. The red cross is the $\ell$=0 experimental value for $J_{max} = 1/2^+$ [5].

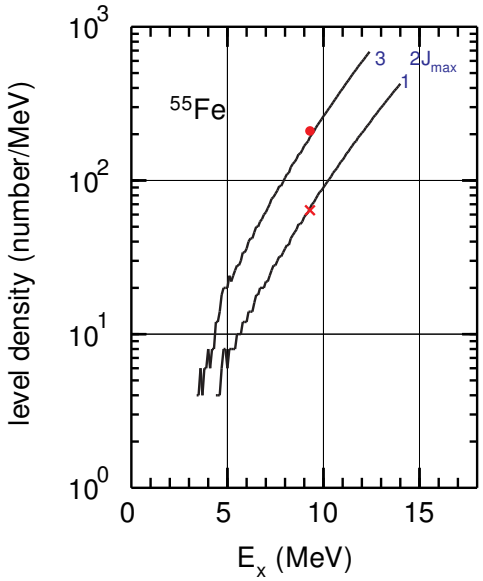


**Fig. 7:** Level density for negative parity states calculated for $^{55}$Fe up to $J_{max} = 3/2^-$. The lines show the cumulative level density up to the value of $2J_{max}$ as indicated on the right-hand side. The red dot is the $\ell$=1 experimental value [5] for $J_{max} = 3/2^-$ at the neutron separation energy. The red cross is the $\ell$=0 experimental value [5] for $J_{max} = 1/2^+$.

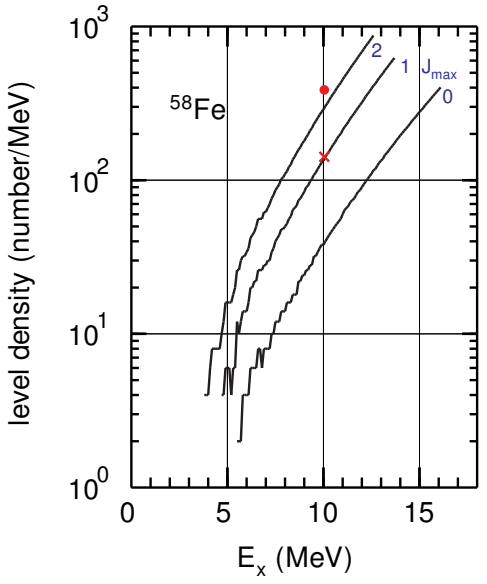


**Fig. 8:** Level density for positive parity states calculated for $^{58}$Fe up to $J_{max} = 2$. The lines show the cumulative level density up to the value of $J_{max}$ as indicated on the right-hand side. The red dot is the $\ell$=1 experimental value [5] for $J_{max} = 2^+$ at the neutron separation energy. The red cross is the $\ell$=0 experimental value [5] for $J_{max} = 1^-$.

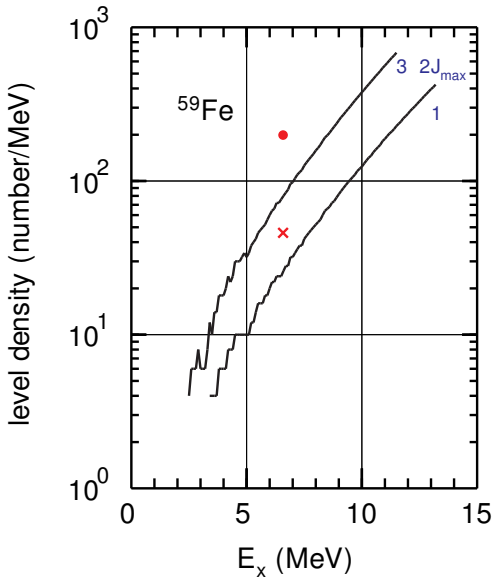


**Fig. 9:** Level density for negative parity states calculated for $^{57}$Fe up to $2J_{max} = 3$. The lines show the cumulative level density up to the value of $2J_{max}$ as indicated on the right-hand side. The red dot is the $\ell$=1 experimental value [5] for $J_{max} = 3/2^-$ at the neutron separation energy. The red cross is the $\ell$=0 experimental value [5] for $J_{max} = 1/2^+$.

The next step is to improve the extrapolation by adding adding higher polynomials in $z_i$. There are several options for this, but based on the comparison to the exact calculations we propose

$$\alpha_i = a_0 + a_2\, z_i^2 \quad \text{and} \quad \beta_i^2 = b_1\, z_i + b_2\, z_i^2. \tag{4}$$

The first and second moments from these equations are

$$H_1 = a_0 + 2a_2 \quad \text{and} \quad M_2 = -2b_1 + 4b_2 \tag{5}$$

(the contribution of $a_2$ to $M_2$ can be neglected). From the exact results in Fig. 1 one observes that the coefficients of the two extra terms can be obtained from the exact calculation in the region around $i_f = 75$. We calculate the average $< \alpha >$ and $< \beta^2 >$ over the interval of iterations from 50 to 100. Then from the equations

$$\alpha_1 = a_0 + 2a_2 \quad \text{and} \quad < \alpha > = a_0 + a_2\, z_f^2, \tag{6}$$

we obtain $a_0$ and $a_2$. And from the equations

$$\beta_1^2 = -2b_1 + 4b_2 \quad \text{and} \quad < \beta^2 > = b_1\, z_f + b_2\, z_f^2, \tag{7}$$

we obtain $b_1$ and $b_2$. The results for $^{48}$Cr are shown in Fig. 2. Our extrapolated Lanzcos matrix method, ELM($i_c$), is to use the exact TDME up to some value $i_c$, and then to use the extrapolations based on the ELM above $i_c$. This large tri-diagonal matrix is then diagaonalized to obtain an approximation for the energies. For example, if we want 1000 energies in the approximation we need to diagonalize the ELM with a dimension of about dimension of about 15,000. The results for ELM(100) for the level density of $^{48}$Cr are shown in the bottom of Fig. 2 and compared to the exact results. The agreement between the two is excellent.

Next we consider the case of $^{57}$Fe. The NuShellX code is usually used with a Hamiltonian such as GPFX1A to study the low lying states. In full $pf$ shell basis all states have negative parity and the $M$-scheme dimension is 455,078,656. In the proton-neutron basis of NuShellX this $M$-scheme dimension is divided among $J$-scheme dimensions for all possible $J$ values. For the study of low-lying states one typically needs to have converged eigenvectors for the lowest 10 states and this requires about 150 Lanczos iterations for each $J$. The low-lying level scheme obtained from this calculation is compared to experiment in Fig. 3. There is a good agreement with theory with known negative parity states. The positive parity states start with the 9/2$^+$ at 2.46 MeV.

Our goal with the ELM method is to use the information obtained during the calculation for 10 converged low-lying states for each $J$ value to make an extrapolation for the level density for up to several thousand states. We consider the case for $J^\pi = 3/2^-$ with a dimension of $N_{dim} = 25,743,302$. In order to compare the ELM method with a more complete calculation, we carried out about 1000 iterations. The results are shown in Fig. 4, where the TDME for the 1000 iterations (black) is compared to the ELM(100) approximation (red). The black line in the bottom panel shows the result of diagonalizing the TDME with a dimension of 1000. It shows the expected result that about 70 levels are converged in energy. Above that, the states no longer increase in density, but become equally spaced (the "picket-fence" type spacing). The ELM(100) level density follows the exact result up to about 70, but after that it continues to increase nearly exponentially.

We can compare the level density to experiment in two ways. First for the cumulative number of levels. The theoretical results are compared to experiment in Fig. 5. As expected, the theory and experiment agree well up to about 2 MeV. From 2-4 MeV there are more levels in experiment. That can be interpreted as the extra contribution of positive parity states. Above 6 MeV the experimental level information is incomplete and the data fall off compared to the theory.

The other type of information is from the level densities for resonances with $\ell$=0 and $\ell$=1 obtained from neutron scattering experiments for energies near the one-neutron separation energy. The experimental values for the level spacing $D_0$ ($\ell$=0) and $D_1$ ($\ell$=1) are given in [5]. These are used to obtain the

average level density, $\rho_\ell = 1/D_\ell$. For $^{55,57,59}$Fe the neutron targets of $^{54,56,58}$Fe have $J_i = 0^+$, and the $\ell$=1 final states are 1/2$^-$ ($p_{1/2}$) and 3/2$^-$ ($p_{3/2}$). For $^{58}$Fe the neutron target of $^{57}$Fe has $J_i = 1/2^-$, and the $\ell$=1 final states are (0,1,2)$^+$.

The level density in $^{57}$Fe for all $J^-$ states up to 19/2$^-$ is shown in Fig. 6. The contribution to the level density up to 15 MeV for higher $J$ values is negligible. The calculation is in perfect agreement with the experimental value [5] for $J_{max} = 3/2^-$ at $E_x = S_n = 7.65$ MeV (red circle). The results for states reached by $\ell$=1 are shown for $^{55}$Fe (Fig. 7), $^{58}$Fe (Fig. 8), and $^{59}$Fe (Fig. 9). The comparison with experiment [5] for $\ell$=1 resonances is excellent for $^{55,57,58}$Fe. For $^{59}$Fe the experimental level density for $\ell$=1 at $S_n = 6.58$ MeV is about a factor of three larger than that calculated. If the experiment is correct, it indicates that model space must be expanded to include the the neutron $0g_{9/2}$ orbital. For all nuclei at higher excitation energy, the experimental level density for negative-parity states must become larger than that calculated due to the truncation to the $pf$ model space.

For $^{57}$Fe, experimental $\ell$=0 level density for 1/2$^+$ states (red cross) [5] is close to the calculated level density value for the 1/2$^-$ states. This indicates that the parity ratio for the level density at this excitation energy is near unity at $E_x = 7.65$ MeV. This information together with that in Fig. 5 indicates that the positive to negative parity level density ratio increases from zero at low excitation energy to about one at $E_x = 7.65$ MeV.

The calculation for the 1/2$^+$ level density must take into account particle and hole excitations beyond the $pf$ model space. For example, for $^{57}$Fe we should consider the coupling of the $\nu(0g_{9/2})$ particle orbital to the calculated level density of (4,5)$^+$ states of $^{56}$Fe, and the coupling of $\pi(0d_{3/2}, 1s_{1/2})$ hole orbitals to the calculated level density of (0,1,2,3)$^+$ states of $^{58}$Co. This is a possible future extension.

Another extension of this work will be to consider the constraints on the polynomial expansion coefficients of Eq. 4 based upon higher moments from $\alpha_2$, $\alpha_3$, $\beta_2$ .... There will be many applications of this new method with regard to comparison with experimental data and other level density models. We can compare our result to those of the moments method [9] to constrain the eta parameter in that model.

**Acknowledgments** This work is partly supported by NSF grant PHY-1811855, and under the auspices of the U.S. Department of Energy by Lawrence Livermore National Laboratory under Contract DE-AC52-07NA27344

## References

[1] M. Burbidge, G. Burbidge, W. Fowler, and F. Hoyle, Rev. Mod. Phys. 29, 547 (1957).

[2] D. Kasen, B. Metzger, J. Barnes, E. Quataert, and E. Ramirez-Ruiz, Nature Vol. **551**, 80 (2017).

[3] J. E. Escher, J. T. Burke, F. S. Dietrich, N. D. Scielzo, I. J. Thompson, W. Younes, Rev. Mod. Phys. **84**, 353 (2012).

[4] C. Lanczos, J. Res. Nat. Bur. Stand. **45**, 252 (1950); J. H. Wilkinson, *The Algebraic Eigenvalue Problem*, (Clarendon, Oxford, 1965).

[5] Atlas of Neutron Resonances Volume 1: Resonance Properties and Thermal Cross Sections Z= 1-60 by Said F. Mughabghab, Elsevier (2018) (doi.org/10.1016/B978-0-44-463769-7.00001-4).

[6] A.P. Zuker, L. Waha Ndeuna, F. Nowacki, and E. Caurier, Phys. Rev. C bf 64, 021394(R) (2001); E. Caurier, G. Martinez-Pinedo, F. Nowacki, A. Poves, A.P. Zuker, rev. Mod. Phys. **77**, 427 (2005).

[7] B. A. Brown and W. D. M. Rae, Nuclear Data Sheets **120**, 115 (2014).

[8] M. Honma, T. Otsuka, B.A. Brown and T. Mizusaki, Euro. Phys. Jour. A **25** Suppl. 1, 499 (2005).

[9] R. A. Sen'kov and M. Horoi, Phys. Rev. C **82**, 024304 (2010); R. A. Sen'kov, M. Horoi, and V. G. Zelivinsky, Comp. Phys. Comm. **184**, 215 (2013).